UKF-Based Model Parameter Estimation to Localize the Seizure Onset Zone in ECoG

Junfeng Lu, Donghui Zhang, Kunlin Guo, Kunying Meng, Denghai Wang, Kai Lu, Renping Yu, Lifang Yang, Mengmeng Li, Rui Zhang, Hong Wan, and Mingming Chen

***Abstract*—Drug-resistant epilepsy (DRE) patients typically require surgical intervention or neurostimulation. Therefore, accurate localization of the seizure onset zone (SOZ) is essential for effective clinical intervention. Although some physiologically meaningful parameters of neural computational models show substantial differences across brain regions during seizures, few studies pay attention to applying these model parameters to SOZ localization. To investigate whether the parameter can be used for accurate SOZ localization, the unscented kalman filter (UKF) is employed to estimate the excitatory-inhibitory balance parameter c from the Z6 neural computational model using DRE patients' electrocorticography (ECoG). The results indicate that this parameter follows a unimodal distribution during the pre-ictal period and the post-ictal period, while exhibiting a bimodal distribution during the ictal period. Then, the distribution of this parameter is combined with machine learning methods, and a bagged tree classifier is constructed to localize the SOZ. The classification results demonstrate that the classifier based on parameter distributions exhibits excellent performance, particularly during the post-ictal period, with an average accuracy of 91.60% . Interestingly, SOZ localization is more accurate when no lesions are detected on magnetic resonance imaging (MRI) compared to when lesions are present. Finally, the model parameter distributions of the SOZs are utilized to predict the outcome of epilepsy surgery. Of note, the results demonstrate that the parameter distribution accurately predicts surgical outcomes with an average accuracy of 92.56% . These findings suggest that the distribution of neural computational model parameters may serve as biomarkers for SOZ localization and epilepsy surgery outcome prediction, providing valuable support and assistance for clinical decision-making.**

***Index Terms*—Drug-resistant epilepsy, ECoG, parameter distribution, machine learning, seizure onset zone (SOZ) localization.**

I. Introduction

EPILEPSY is a chronic neurological disorder caused by abnormal electrical discharges in brain neurons, characterized by recurrent seizures [1]. The impact of epilepsy extends beyond the physical harm experienced during seizures, encompassing long-term psychological and cognitive effects as well [2], [3]. Currently, antiepileptic drugs are the most commonly used treatment for epilepsy. However, approximately 30% of patients are unable to achieve effective seizure control through medication alone, and this type of epilepsy is known as drug-resistant epilepsy (DRE) [4]. With the deepening understanding of epilepsy, surgical interventions and neurostimulation therapies have become feasible options for DRE patients [5], [6]. In the clinical diagnosis and treatment of epilepsy, particularly in surgical interventions for DRE, accurately identifying the seizure onset zone (SOZ) is crucial for developing a surgical plan and preserving the patient's neurological functions [7], [8].

Currently, researchers have proposed various strategies and tools for localizing SOZ through analysis of electroencephalography (EEG), including methods such as neural fragility [9], cross-frequency coupling [10], high-frequency oscillations [11], and dynamic networks [12], which have played a critical role in clinical pre-surgical evaluations and treatment decision-making. In recent years, as intracranial electroencephalography (iEEG) offers higher spatial resolution, better signal quality, and coverage of deep brain regions [13], researchers have increasingly employed iEEG, or combined EEG with iEEG, to study epilepsy, showing great potential for SOZ localization. iEEG encompasses two primary techniques: electrocorticography (ECoG) and stereo-electroencephalography (SEEG) [14]. Specifically, ECoG records brain activity by placing electrode grids or strips directly on the cortical surface, while SEEG employs depth electrodes implanted in the brain to capture electrical activity from deep brain structures. Despite these advances, many of these studies do not provide a clear and comprehensive representation of the underlying excitatory and inhibitory processes occurring in the brain during seizures, which are crucial for understanding seizure dynamics and SOZ localization.

Beyond studies based on clinical experimental data, researchers often explore the physiological mechanisms of neu-

Received 14 September 2024; revised 23 January 2025; accepted 16 May 2025. Date of publication 21 May 2025; date of current version 9 September 2025. This work was supported in part by the National Natural Science Foundation of China under Grant 62173310, in part by MOST 2030 Brain Project under Project 2022ZD0208500, and in part by the Technology Project of Henan Province under Grant 242102311015 and Grant 222102310031. *(Corresponding authors: Hong Wan; Mingming Chen.)*

All ECoG data used in this article are acquired from the HUP iEEG Epilepsy Dataset (https://openneuro.org/datasets/ds004100/versions/1.1.3).

The authors are with the Henan Key Laboratory of Brain Science and Brain–Computer Interface Technology, School of Electrical and Information Engineering, Zhengzhou University, Zhengzhou 450001, China (e-mail: wanhong@zzu.edu.cn; mmchen@zzu.edu.cn).

Digital Object Identifier 10.1109/JBHI.2025.3572204

rological disorders such as epilepsy from the perspective of neural computational models. These models can dynamically simulate the real-time changes in brain activity, with several model parameters having electrophysiological significance, and their adjustment allows for fitting complex electrophysiological signals. Neurophysiologically, it has been well established that significant changes in both excitability and inhibition occur during the epileptic evolution [15], [16]. Moreover, there are distinct differences in the excitability of SOZs compared to other brain regions [17], [18]. Hence, neural computational model parameters reflecting physiological states, such as excitability, hold potential as biomarkers for SOZ localization. Integrating these computational models with clinically recorded EEG or ECoG signals, and accurately estimating the model parameters from neural signals, is crucial for SOZ localization.

In recent years, various methods have been applied to parameter estimation in differential models, such as the least squares method [19], genetic algorithms [20], Bayesian optimization [21], Kalman filter (KF) [22], and variational inference [23]. Compared to traditional Kalman filtering methods, the unscented kalman filter (UKF) is better suited for handling highly nonlinear problems and can dynamically capture changes in neural signals in real time. These characteristics make it particularly advantageous for neural computational models, such as the JR model [24] and the Wendling model [25], especially when managing complex dynamic parameters. The parameters estimated by UKF in neural computational models have numerous applications, such as detecting epileptic seizures [26], developing control strategies for epilepsy [27], and exploring the mechanisms of seizure onset and propagation [28]. However, despite the extensive use of model parameters in epilepsy research, few studies have employed these parameters for the localization of the SOZ.

This study aims to combine the excitatory-inhibitory balance parameter in a neural computational model estimated by the UKF with machine learning algorithms to achieve high-performance of SOZ localization, thereby to provide effective support for decision-making in clinical epilepsy surgery. First, UKF is used to estimate the parameters of the simulated epileptic-like signals. The estimated parameters exhibit a high degree of consistency with the preset parameters, demonstrating the feasibility of utilizing UKF in neural signal parameter estimation. Subsequently, UKF is applied to estimate the model parameters with ECoG collected from DRE patients, and the parameter distributions are used as features to build a bagged tree classifier model for SOZ localization. The results indicate that the model performs well in the three periods, with better classification performance in the post-ictal period. In the post-ictal period, the accuracy is 91.60%, and the area under the curve (AUC) is 96.43% . Further analysis shows that SOZ classification improves significantly in patients without magnetic resonance imaging (MRI) lesion status compared to those with lesions. More importantly, the model can successfully predict surgical outcomes based on SOZ parameter distributions, achieving an accuracy of 92.56% . These findings suggest that the distribution of model parameters could serve as a potential biomarker for SOZ localization, providing auxiliary support for medical decision-making in epilepsy.

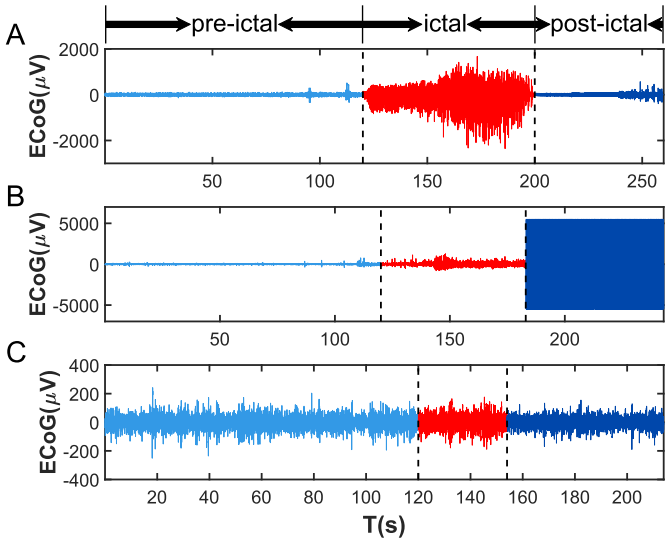

Fig. 1. Examples of selected and excluded ECoG channels. The light blue, red, and dark blue curves represent the ECoG signals during the pre-ictal, ictal, and post-ictal periods, respectively. The black dashed lines indicate the boundaries between different seizure periods. A, a selected channel. B, an excluded channel with obvious defects. C, an excluded SOZ without significant seizure characteristics.

II. Materials and Methods

A. ECoG Data and Preprocessing

The ECoG data used in this work are acquired from the HUP iEEG Epilepsy Dataset created by the Hospital of the University of Pennsylvania (https://openneuro.org/datasets/ds004100) [29]. This dataset includes preoperative intracranial electroencephalography (iEEG) recordings from 58 DRE patients, comprising ECoG from 20 DRE patients and SEEG from 38 DRE patients. Specifically, the reference montage with a reference electrode which is far away from the SOZ is employed to record the ECoG, and the sampling rate is either 500 Hz or 512 Hz. The dataset provides clinically-determined seizure onset channels, as well as channels overlapping with the resection/ablation zone, which are strictly determined by segmenting the resection cavity. In addition, the dataset includes detailed patient information such as lesion status on MRI and Engel surgical outcomes after surgery [30].

In this study, the ECoG data from 20 DRE patients are analyzed. To ensure the reliability of the data, two types of channels are excluded, as shown in Fig. 1: (1) channels with obvious defects in the data, or (2) SOZs that do not show significant seizure characteristics. Specifically, SOZs are excluded if the mean absolute value of the ictal data is less than the mean absolute value plus one standard deviation from the pre-ictal (or post-ictal) period. Of note, if more than half of the SOZs in a single seizure are excluded, that seizure is excluded from the analysis. Ultimately, we selected 17 patients (a total of 47 seizures). The detailed clinical characteristics of these patients are shown in Table I. Here, an Engel grade of 1 indicates a successful epilepsy surgery outcome, whereas an Engel grade greater than 2 indicates a failed outcome.

Subsequently, the selected raw ECoG data are preprocessed using the EEGLAB toolbox [31]. First, the average reference

TABLE I
THE CLINICAL CHARACTERISTICS OF DRE PATIENTS

Characteristic	Statistics
Age(year)	36.29±10.91
Sex(female/male)	10/7
Handedness(right/left/ambidextrous)	5/8/4
Engel($1/2^+$)	13/4
Lesion status on MRI(lesional/non-lesional)	9/8
Age of onset of epilepsy(year)	20.29±13.99
Total seizures	47
Number of SOZs per seizure	7.21±4.93

method is utilized to the raw ECoG to re-reference the data and reduce noise interference. Then, the ECoG data are band-pass filtered in the range of 0.5-45 Hz. Next, the preprocessed ECoG data are segmented based on the seizures marked by time labels. Notably, the first 10 seconds of data are discarded. To ensure uniform data length across different periods, the data in the pre-ictal and post-ictal periods are aligned with the data length in the ictal period. Additionally, given the significant imbalance in ECoG data between SOZ and NSOZ, dimensionality reduction is applied to the parameter distribution characteristics, as described in Section II-E. Feature dimensionality reduction is performed using Python 3.11, while all other data analysis and processing are performed in MATLAB 2021a.

It should be noted that the SOZs for all patients in this dataset are determined and labeled by clinical professionals. Additionally, channels marked as "n/a" in the dataset are defined as non-SOZs (NSOZs).

B. Neural Computational Model

It has been widely demonstrated that the Z6 model, a phenomenal oscillator model, can simulate neural activities observed in the brain, especially, epileptic neural dynamics [32]. The Z6 model is a nonlinear dynamical system defined by an ordinary differential equation [33]:

$$\frac{d}{dt}Z = a|Z|^4 Z + b|Z|^2 Z + cZ + i\omega Z + \eta(t), \qquad (1)$$

Where $Z = x + iy$ is a complex variable, corresponding to the real and imaginary parts of Z, with the real part being used to represent EEG signals. a, b, c, ω are real parameters and $\eta(t)$ is additive noise.

Although the model described by (1) does not involve specific biological mechanisms or processes within neuronal populations, some parameters can be interpreted as "quasi-realistic quantities" with electrophysiological significance [34]. The parameter $a < 0$ prevents the system from infinite activation, the parameter $b > 0$ is related to the generation of action potentials in neuronal populations, the parameter c represents the balance of excitatory and inhibitory activities within neuronal populations, and the parameter $\omega > 0$ indicates the angular velocity of the rotator [32]. Of note, the parameter c is a very important control parameter of the system, and its variation can reflect changes in excitatory and inhibitory activities within a brain region. As c varies, the system transitions between different dynamical states, including stable states, bistability, and limit cycles, exhibiting rich dynamical properties. In the current study, the UKF is utilized to estimate parameter c. According to the previous study that introduced the Z6 model, the default values for parameters a, b, and η are -1, 2, and 0.1, respectively [33]. Notably, since the average peak frequency of ECoG signals from all epilepsy patients is approximately 8 Hz, the parameter ω is set to $2 \times \pi \times 8$. The specific parameters are detailed in Table II.

TABLE II
PARAMETER VALUES OF Z6 MODEL

Parameter	Value
a	-1
b	2
ω	$2 \times \pi \times 8$
η	0.1

C. UKF Algorithm

The UKF is an enhanced Kalman filter algorithm designed for state and parameter estimation in nonlinear systems [35]. By incorporating the Unscented Transformation (UT), the UKF effectively handles the state updates for nonlinear systems [24]. Compared with traditional Kalman filter, UKF is better suited to handle highly nonlinear problems and can capture changes in neural signals in real-time, making it particularly advantageous for neural computational models, especially when dealing with complex dynamic parameters. Assuming the nonlinear dynamic system is described as:

$$\begin{cases} x_k = f(x_{k-1}) + \omega_k \\ y_k = h(x_k) + v_k \end{cases} \qquad (2)$$

Where x_k represents the system state vector at time k, y_k represents the system observation vector at time k, f is the state function, h is the observation function, ω_k is the process noise at time k, and v_k is the observation noise at time k. Both ω and v are independent and follow zero-mean Gaussian distributions.

The specific filtering steps are as follows:

1) Initialization:

$$\begin{cases} \hat{x}_0 = E(x_0) \\ P_0 = E\left((x_0 - \hat{x}_0)(x_0 - \hat{x}_0)^T\right) \end{cases} \qquad (3)$$

Where $\hat{x}_0$ is the initial estimate of the state vector and P_0 represents the initial estimate covariance matrix.

2) Calculation of sigma points:

$$\begin{cases} \chi_{k-1}^{0} = \hat{x}_{k-1} \\ \chi_{k-1}^{i} = \hat{x}_{k-1} \\ \quad + \left(\sqrt{(n+\lambda)P_{k-1}}\right)_i & i = 1, \ldots, L \\ \chi_{k-1}^{i} = \hat{x}_{k-1} \\ \quad - \left(\sqrt{(n+\lambda)P_{k-1}}\right)_i & i = n+1, \ldots, 2L \\ W_0^m = \frac{\lambda}{L+\lambda} \\ W_0^c = \frac{\lambda}{L+\lambda} + (1-\alpha^2+\beta) \\ W_i^m = W_i^c = \frac{1}{2(L+\lambda)} & i = n+1, \ldots, 2L \end{cases} \tag{4}$$

For a random variable x with dimension L, a matrix χ containing $(2L+1)$ sigma vectors χ^i (with corresponding weights W^i) is generated. λ is a scaling parameter, calculated as $\lambda = \alpha^2(L+\kappa) - L$. α determines the spread of the sigma points around $\hat{x}$ and is usually set to a small positive value (e.g., 10^{-3}). κ is a secondary scaling parameter, typically set to 0. β incorporates prior knowledge of the distribution of x (for a Gaussian distribution, $\beta = 2$ is optimal).

3) State prediction:

$$\begin{cases} \chi_{k|k-1}^{i} = f(\chi_{k-1}^{i}) \\ \hat{x}_{k|k-1} = \sum_{i=0}^{2n} W_i^m \chi_{k|k-1}^{i} \\ P_{x,k|k-1} = \sum_{i=0}^{2n} W_i^c \left[\chi_{k|k-1}^{i} - \hat{x}_{k|k-1}\right] \\ \left[\chi_{k|k-1}^{i} - \hat{x}_{k|k-1}\right]^T \\ +Q_k \\ \gamma_{k|k-1}^{i} = h(\gamma_{k-1}^{i}) \\ \hat{y}_{k|k-1} = \sum_{i=0}^{2n} W_i^m \gamma_{k|k-1}^{i} \end{cases} \tag{5}$$

Where Q_k represents the covariance of the process noise ω at time k.

4) Measurement update:

$$\begin{cases} P_{y,k} = \sum_{i=0}^{2n} W_i^c \left[\gamma_{k|k-1}^{i} - \hat{y}_{k|k-1}\right] \\ \left[\gamma_{k|k-1}^{i} - \hat{y}_{k|k-1}\right]^T + R_k \\ P_{xy,k} = \sum_{i=0}^{2n} W_i^c \left[\chi_{k|k-1}^{i} - \hat{x}_{k|k-1}\right] \\ \left[\gamma_{k|k-1}^{i} - \hat{y}_{k|k-1}\right]^T \\ K = P_{xy,k} P_{y,k}^{-1} \\ \hat{x}_k = \hat{x}_{k|k-1} + K\left(y_k - \hat{y}_{k|k-1}\right) \\ P_{x,k} = P_{x,k|k-1} - K P_{y,k} K^T \end{cases} \tag{6}$$

Where R_k represents the covariance of the observation noise v at time k. K represents the Kalman gain in UKF.

Notably, $\hat{x}_k = [\hat{xx}_k, \hat{xy}_k, \hat{xc}_k]$ is a 3× 1 vector, representing the real part, imaginary part, and parameter c of the Z6 model's output at time k, respectively, while y_k is the ECoG signal value at time k. By inputting a vector $Y = [y_1, y_2, \ldots, y_k, \ldots, y_T]$ $(k = 1, 2, \ldots, T)$ into the UKF system, three output vectors are obtained: $\hat{Xx} = [\hat{xx}_1, \hat{xx}_2, \ldots, \hat{xx}_k, \ldots, \hat{xx}_T](k = 1, 2, \ldots, T)$, $\hat{Xy} = [\hat{xy}_1, \hat{xy}_2, \ldots, \hat{xy}_k, \ldots, \hat{xy}_T](k = 1, 2, \ldots, T)$ and $\hat{Xc} = [\hat{xc}_1, \hat{xc}_2, \ldots, \hat{xc}_k, \ldots, \hat{xc}_T](k = 1, 2, \ldots, T)$, where the vector $\hat{Xc}$ represents the sequence of parameter c corresponding to the ECoG signal over time period T.

In the current study, to remove external noise and ensure the reliability of parameter estimation, the first and last 5 seconds of ECoG are excluded. Additionally, to minimize the root mean square error (RMSE) between the true and output signals, the process noise covariance in the UKF is empirically set to $Q = \text{diag}(0.06, 0.06, 0.02)$ and the observation noise covariance is set to $R = 0.5$. Finally, to facilitate the analysis of model parameters, the parameters for each channel during each seizure are normalized to a range of -1 to 1.

D. Calculation of the Model Parameter Distribution

To quantify the distribution characteristics of the model parameters, the elements of a $1 \times n$ parameter vector $\mathbf{C}$ are divided into a distribution vector using a specified step size. The detailed procedure is as follows:

1) Parameter vector definition: First, all elements of the parameter vector $\mathbf{C}$ are restricted to the interval $[-1, 1]$. The parameter vector is defined as:

$$\mathbf{C} = [c_1, c_2, \ldots, c_n] \tag{7}$$

Where $c_i \in [-1, 1]$.

2) Interval edges definition: The range of vector $\mathbf{C}$ in $[-1, 1]$ is divided into 200 equally spaced intervals. The interval edges are defined as:

$$\text{edges} = [-1, -0.99, -0.98, \ldots, 0.99, 1] \tag{8}$$

3) Calculation of the number of elements: Using the histogram counting method, calculate the number of elements in vector $\mathbf{C}$ that fall within each interval, resulting in a vector $\mathbf{H}$:

$$\mathbf{H} = \text{histcounts}(\mathbf{C}, \text{edges}) \tag{9}$$

The resulting vector $\mathbf{H}$ is a 1×200 vector that represents the distribution of elements in the parameter vector $\mathbf{C}$ across the interval $[-1, 1]$.

E. SOZ Localization Based on Parameter Distribution

To localize the SOZ, the model parameter of epileptic signals estimated by UKF is used as features for classifying SOZ and NSOZ. Note that the data are collected from patients who underwent successful epilepsy surgery, including ECoG from both SOZ and NSOZ. To effectively extract features, the UKF is used to estimate model parameters from these signals. For a segment of ECoG signal with T sampling points, T parameters c can be estimated. These T parameters are then distributed into 200 equally spaced intervals within the range $[-1, 1]$, resulting in a $1\times$ 200 parameter distribution vector, which is used as the input to the classification model. To classify SOZ and NSOZ, the bagged trees classifier is employed. Bagged trees is an ensemble learning method that enhances classification accuracy and robustness by training multiple decision trees and aggregating their outputs. The advantage of bagged trees lies in its ability to reduce the variance of individual decision trees, thereby improving model stability and generalization [36]. However, there is a significant imbalance in the ECoG data between SOZ and NSOZ, with

248 and 2525 cases, respectively. Here,to address this imbalance, we adopt the method proposed by Lemaitre Guillaume et al. [37], which involves techniques such as under-sampling, over-sampling, and generating synthetic samples to balance the dataset across classes. This approach prevents the classifier from being biased towards the majority class. For the classification model training, the dataset is randomly split into training and testing sets at an 8:2 ratio, and this process is repeated 100 times. To comprehensively evaluate the performance of the classifier, four metrics are used: $Accuracy$, $Sensitivity$, $Specificity$, and the Area Under the ROC Curve (AUC) [38]. These metrics are calculated as follows:

$$Accuracy = \frac{TP + TN}{TP + FP + TN + FN} \tag{10}$$

$$Sensitivity = \frac{TP}{TP + FN} \tag{11}$$

$$Specificity = \frac{TN}{TN + FP} \tag{12}$$

Where TP represents true positives, TN represents true negatives, FP represents false positives, and FN represents false negatives.

Next, to investigate the potential impact of different MRI lesion states on SOZ localization, the parameter distributions under various MRI lesion conditions are obtained. Specifically, the patients are divided into two groups: one group with lesions visible on MRI and another without visible lesions. Classification of SOZ and NSOZ is then performed separately for each group.

F. Surgical Outcome Prediction Based on Parameter Distribution

The current study further explores the potential of predicting surgical outcomes by analyzing the distribution of model parameters derived from epilepsy patients. As mentioned above, the data come from a cohort of postoperative epilepsy patients, with some achieving successful outcomes and others experiencing unsuccessful surgeries. Of note, model parameters are extracted from the ECoG data in the SOZ, with the data segmented into pre-ictal, ictal and post-ictal periods. The distribution of these model parameters is used as a feature to classify and predict whether the surgical outcome is successful or not.

Similar to the previous analysis, the data of patients with successful surgeries greatly outnumber those with unsuccessful outcomes. To address this imbalance, a previously mentioned imbalanced learning method is employed [37]. The bagged trees classifier is used again, with the dataset randomly split into training and testing sets at an 8:2 ratio, repeated 100 times. To evaluate the ability of the model parameter distribution to predict surgical outcomes, the mean and standard deviation of the accuracy, sensitivity, specificity, and AUC from these 100 iterations are calculated and reported. Finally, rank-sum tests are performed to evaluate the accuracy and other metrics of SOZ localization results across different periods and MRI lesion conditions, as well as surgical outcome predictions across different periods. $P<0.05$ is considered statistically significant.

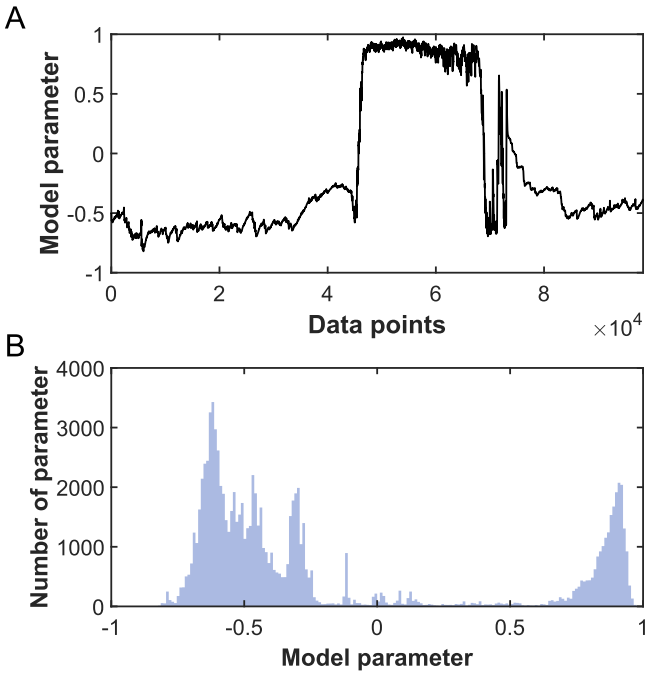

Fig. 2. An example showing the distribution of model parameter. A, original parameter. B, distribution of parameter values.

III. Results

A. UKF-Based Model Parameter Estimation of Simulated Epileptic-Like Signals

Theoretically, the parameter c in the Z6 model can represent the relative balance between the excitability and inhibition of neuron masses. Therefore, the value of the parameter c can determine the state of the model's output. To verify this, we set the parameter c in the Z6 model with different values to observe the effect of these changes on the model's output. Note that the other parameters in the Z6 model are fixed at the following values: $a = -1, b = 2, \omega = 2 \times \pi \times 8$, and η is Gaussian white noise with a mean of 1.

Obviously, when the other parameters remain unchanged, different values of the parameter c lead to different model outputs, as shown in Fig. 3. Intuitively, when $c = -8$, the system is in a steady state, and the output signal represents normal brain activity (Fig. 3(a)). When $c = -0.9$, the system is in a bistable state, with both fixed-point and limit-cycle states observable (Fig. 3(b)). And when $c = 8$, the system corresponds to a limit cycle, and the model output exhibits epileptic-like signals (Fig. 3(c)). Theoretically, as the parameter c gradually changes from negative to positive values, the model's output signal transitions from spontaneous brain activity to epileptic-like signals. Conversely, when c changes from positive to negative values, the signal should transmit from epileptic-like signals back to a normal state. Actually, these two processes correspond to the onset and offset of epilepsy. Taken together, these results indicate that the parameter c can determine the system's state in the Z6 model. Therefore, estimating the parameter c is crucial to understand the excitability and inhibition within brain regions.

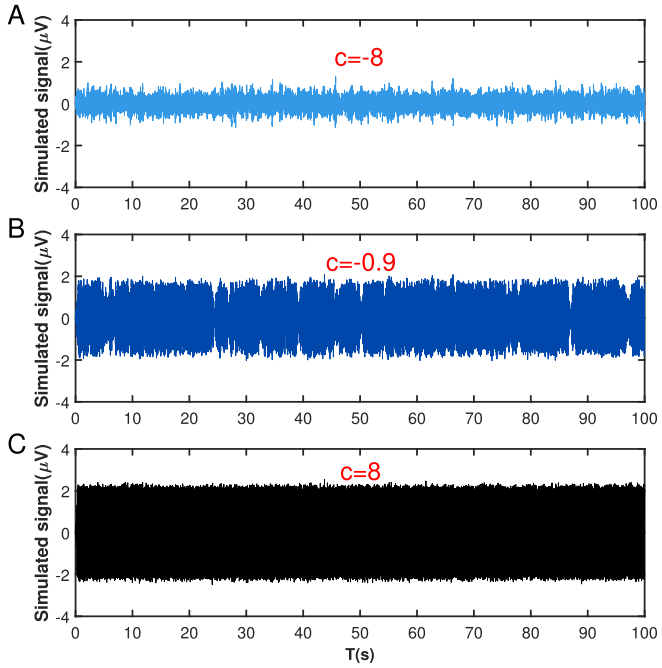

Fig. 3. Simulated signals of Z6 model with different c values. A, c=−8. B, c=−0.9. C, c=8.

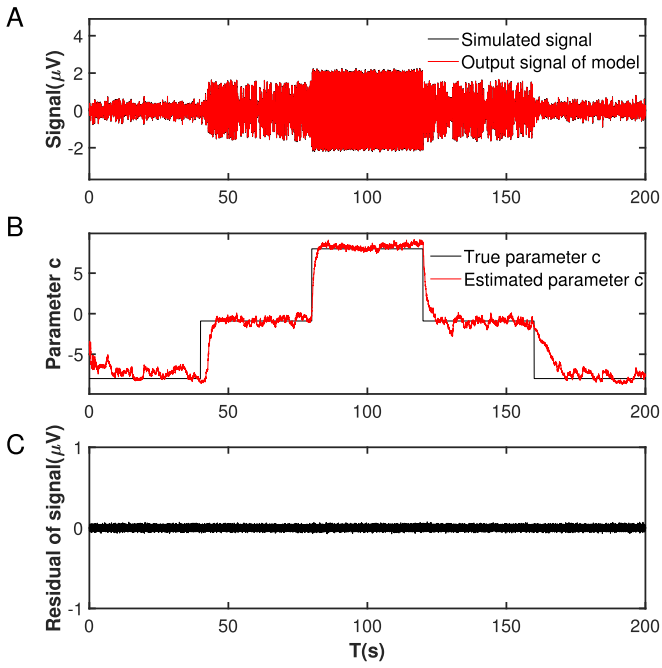

Fig. 4. Parameters estimation of simulated epileptic-like signal. A, the simulated epileptic-like signal. B, the estimated parameter c. C, the residual between simulated and output signals.

To validate the feasibility of the UKF method for estimating model parameters of neural signals, the UKF method is first employed to estimate the model parameters of simulated epileptic signals in this study. Here, the model used is the Z6 model, the neural signals are the simulated epileptic signals (Fig. 4(a)), and the parameter estimated is the balance parameter c of the Z6 model.

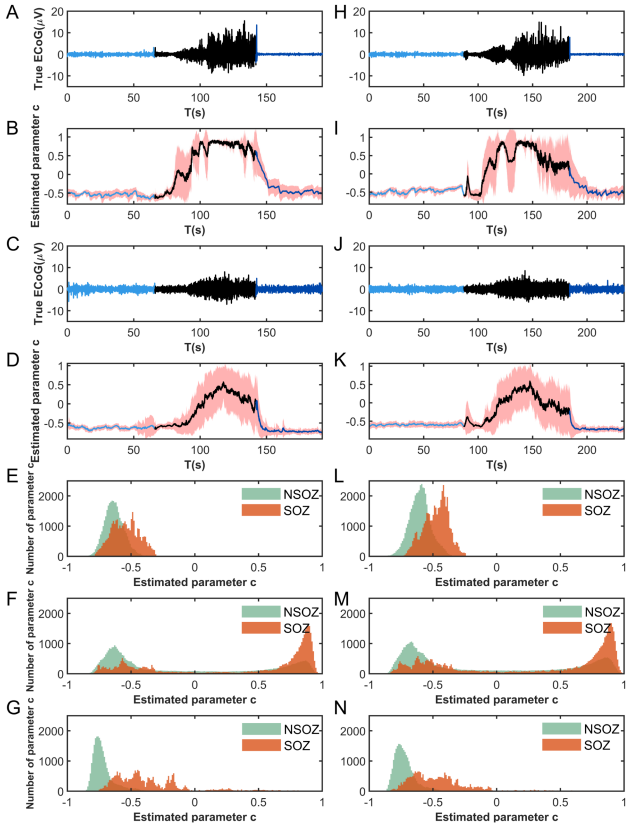

Fig. 5. Model parameters estimation and distribution of true epileptic ECoG in patient HUP074. A, the epileptic ECoG of an SOZ. B, the estimated parameters of all SOZs. C, the epileptic ECoG of an NSOZ. D, the estimated parameters of all NSOZs. E, the mean parameter distribution in the pre-ictal period. F, the mean parameter distribution in the ictal period. G, the mean parameter distribution in the post-ictal period. H-N, the epileptic ECoG, parameter estimation, and distribution of another seizure in patient HUP074. The light blue, black, and dark blue curves represent the ECoG and the mean of the estimated parameters in the pre-ictal, ictal, and post-ictal periods, respectively. The red shading represents the standard deviation of the estimated parameters.

It is observed that as the simulated epileptic-like signal transition between normal and seizure states, the model output signal estimated by the UKF closely matches the simulated signal, with the residual between them remaining near zero during the epileptic phases (Fig. 4). Importantly, the parameter c estimated by the UKF first increases and then decreases, exhibiting the same trend as the true parameter c, and the estimated values consistently remain close to the true values (Fig. 4(b)). Summarily, these results demonstrate that the UKF method performs well in estimating the state and parameters of neural computational models for both normal and epileptic neural signals.

B. Model Parameter Estimation of True Epileptic ECoG Based on UKF

The feasibility of using UKF to estimate model parameters of epileptic-like signals has already been demonstrated. Accordingly, the UKF is further used to estimate the model parameter from the true epileptic ECoG of DRE patients.

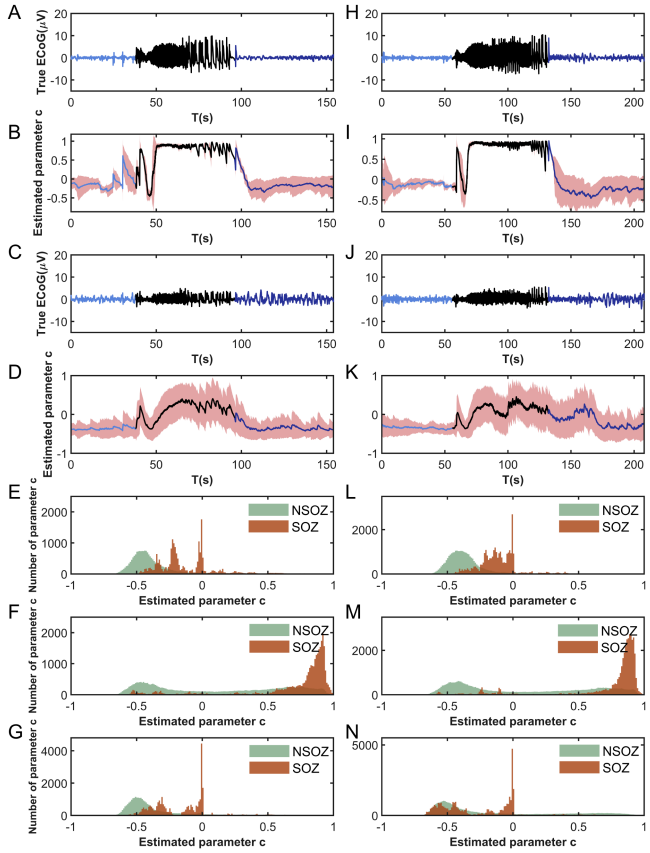

Fig. 6. Model parameters estimation and distribution of true epileptic ECoG in patient HUP126. A, the epileptic ECoG of an SOZ. B, the estimated parameters of all SOZs. C, the epileptic ECoG of an NSOZ. D, the estimated parameters of all NSOZs. E, the mean parameter distribution in the pre-ictal period. F, the mean parameter distribution in the ictal period. G, the mean parameter distribution in the post-ictal period. H-N, the epileptic ECoG, parameter estimation, and distribution of another seizure in patient HUP126. The light blue, black, and dark blue curves represent the ECoG and the mean of the estimated parameters in the pre-ictal, ictal, and post-ictal periods, respectively. The red shading represents the standard deviation of the estimated parameters.

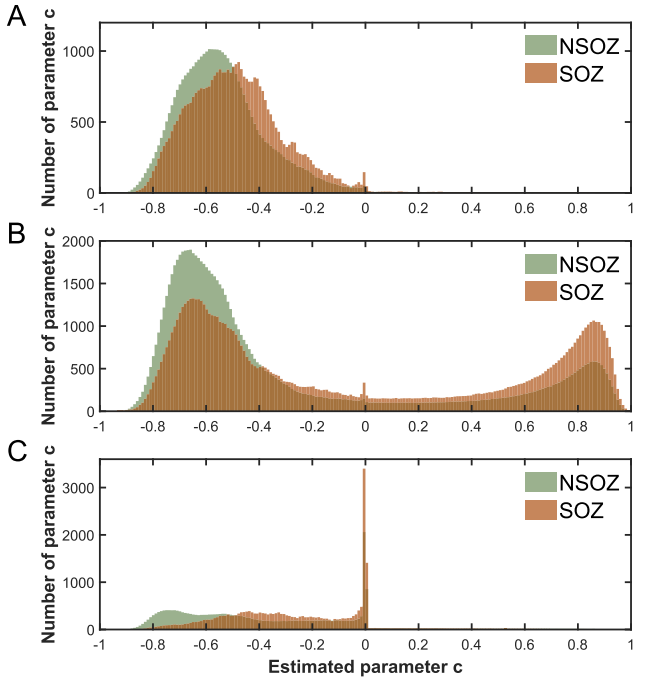

Fig. 7. Model parameters distribution of true epileptic ECoG in all patients. A, the mean parameter distribution in the pre-ictal period. B, the mean parameter distribution in the ictal period. C, the mean parameter distribution in the post-ictal period.

Subsequently, Figs. 5 and 6 show the estimated model parameters and their distributions from two seizures in two DRE patients who undergo successful surgery (HUP074 and HUP126).

As shown in Fig. 5, it can be easily observed that the estimated model parameters initially increase and then decrease during the epileptic evolution for both the SOZ and the NSOZ. Notably, despite the similar overall dynamic trend, the parameter changes in SOZ are significantly larger than those in NSOZ (Fig. 5(b) and (d)).

Further analysis of the parameter distributions indicates that during the pre-ictal period (Fig. 5(e)), both SOZ and NSOZ parameters exhibit a clear unimodal distribution, with the peak parameter in SOZ being higher than that in NSOZ. In contrast, during the ictal period (Fig. 5(f)), both SOZ and NSOZ parameters show a clear bimodal distribution, with peaks in both the negative and positive ranges. Notably, in the negative range, the peak of parameter distribution in NSOZ is higher than that in SOZ, while in the positive range, the peak of parameter distribution in SOZ exceeds that in NSOZ. Additionally, during the postictal period (Fig. 5(g)), the parameters of NSOZ exhibit a distinct unimodal distribution, whereas the parameters of SOZ show a more uniform distribution without a prominent peak. Moreover, the dynamic changes and distribution of the estimated model parameters exhibit the same pattern during another seizure in the same patient (Fig. 5(h) to Fig. 5(n)).

The dynamic changes and distribution of model parameters in patient HUP074 are not isolated cases, similar patterns can also be observed in data from other patients, such as patient HUP126 (Fig. 6). Interestingly, during the pre-ictal period, the difference between the peak parameters of SOZ and NSOZ in patient HUP126 is more pronounced compared to patient HUP074. Moreover, during the ictal period, the parameter distribution in SOZ in HUP126 tends to be more unimodal, even concentrating around 1. And during the post-ictal period, the SOZ parameters of HUP126 exhibit a unimodal distribution, primarily concentrated around 0.

Finally, to verify the generalizability of these observations, a statistical analysis of the model parameter distributions is conducted for all 13 successfully operated DRE patients, as shown in Fig. 7. During the pre-ictal period, the parameter generally follows a unimodal distribution, and the parameter distribution in the SOZ is typically localized to the right of the NSOZ parameter distribution. During the ictal period, the parameter exhibits a bimodal distribution. Notably, the peak in the negative range for SOZ is smaller than that for NSOZ, while in the positive range, the peak for SOZ is greater than that for NSOZ. Additionally, during the post-ictal period, the parameter exhibits a unimodal distribution, peaking around the

TABLE III
SOZ CLASSIFICATION PERFORMANCE BASED ON PARAMETER DISTRIBUTION

periods	accuracy	sensitivity	specificity	AUC
pre-ictal	0.8982± 0.0237	0.9082± 0.0423	0.8883± 0.0424	0.9637± 0.0155
ictal	0.8817± 0.0304	0.8536± 0.0533	**0.9096± 0.0414**	0.9480± 0.0207
post-ictal	**0.9160± 0.0208**	**0.9554± 0.0293**	0.8764± 0.0443	**0.9643± 0.0158**

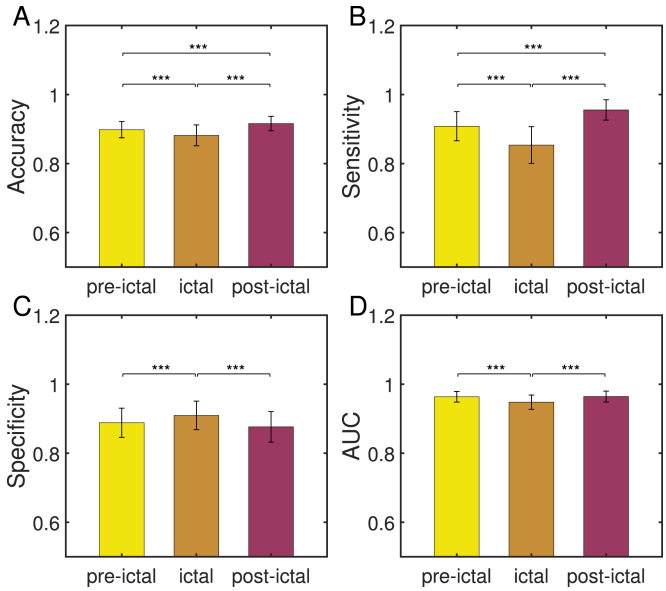

Fig. 8. SOZ classification performance based on parameter distribution. A, Accuracy. B, Sensitivity. C, Specificity. D, AUC. *** indicates $P<0.001$.

TABLE IV
SOZ CLASSIFICATION PERFORMANCE OF DIFFERENT LESION STATUSES ON MRI

periods	lesion status on MRI	accuracy	sensitivity	specificity	AUC
pre-ictal	lesional	0.8678± 0.0335	0.8871± 0.0455	0.8484± 0.0675	0.9415± 0.0237
	non-lesional	**0.9643± 0.0416**	**0.9832± 0.0517**	**0.9454± 0.0666**	0.9828± 0.0298
ictal	lesional	0.8603± 0.0354	0.8295± 0.0585	0.8911± 0.0559	0.9330± 0.0249
	non-lesional	0.8230± 0.0683	0.8556± 0.1221	0.7909± 0.1152	0.8970± 0.0684
post-ictal	lesional	0.8493± 0.0399	0.8942± 0.0525	0.8045± 0.0623	0.9252± 0.0280
	non-lesional	0.9561± 0.0430	0.9723± 0.0586	0.9399± 0.0673	**0.9872± 0.0213**

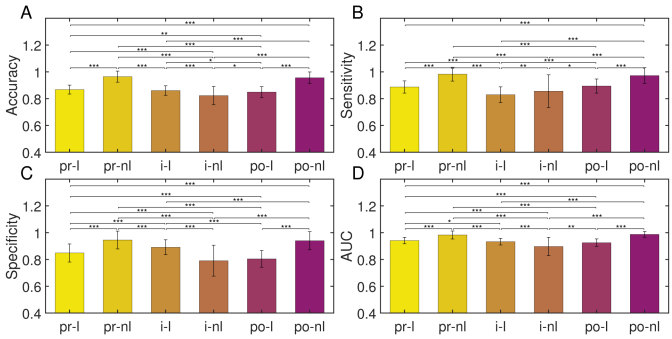

Fig. 9. SOZ classification performance of different lesion statuses on MRI. A, Accuracy. B, Sensitivity. C, Specificity. D, AUC. The abbreviations for classification groups are as follows: pr-l represents pre-ictal and lesional, pr-nl represents pre-ictal and non-lesional, i-l represents ictal and lesional, i-nl represents ictal and non-lesional, po-l represents post-ictal and lesional, and po-nl represents post-ictal and non-lesional. Statistical significance is indicated as follows: * for $P<0.05$, ** for $P<0.01$, and *** for $P<0.001$.

vicinity of 0, and the peak value of SOZ is higher than that of NSOZ. This suggests that despite the heterogeneity among different patients, the observed distribution patterns are valid on a broader scale, providing a reliable basis for further clinical applications.

C. SOZ Localization Based on Model Parameter Distribution

By using the model parameter distributions estimated from the ECoG of patients who undergo successful epilepsy surgery as features, and employing bagged trees as the classifier, classification of SOZs and NSOZs has been performed on 13 DRE patients. The results indicate that the classification performance during the post-ictal period is generally better than that during the pre-ictal and ictal periods, as shown in Tables III and Fig. 8. Intuitively, during the post-ictal period, the classification model achieves significantly higher accuracy (0.9160 ± 0.0208), sensitivity (0.9554 ± 0.0293), and AUC (0.9643 ± 0.0158), whereas during the ictal period, the model exhibits higher specificity (0.9096 ± 0.0414). These findings suggest that combining UKF-based model parameter estimation with machine learning classification algorithms can effectively localize SOZs from the ECoG of epilepsy patients, especially during the post-ictal period.

To further explore the potential impact of MRI lesion status on SOZ localization, the 13 epilepsy patients are divided into an MRI lesion group (9 patients) and a non-lesion group (4 patients), then the SOZ localization analyses are conducted separately for each group. The results show that during the pre-ictal and post-ictal periods, the classification accuracy in the non-lesion group (0.9643 ± 0.0416 and 0.9561 ± 0.0430) is significantly higher than that in the lesion group (0.8678 ± 0.0335 and 0.8493 ± 0.0399). Conversely, during the ictal period, the classification accuracy in the lesion group (0.8603 ± 0.0354) is higher than that in the non-lesion group (0.8230 ± 0.0683), as shown in Table IV and Fig. 9. Overall, the classification accuracy in the pre-ictal non-lesion group and post-ictal non-lesion group is significantly higher than that in other conditions. Additionally, during the pre-ictal and post-ictal periods, the non-lesion group also exhibits higher sensitivity (0.9832 ± 0.0517 and 0.9723 ± 0.0586),

TABLE V
SURGICAL OUTCOMES CLASSIFICATION PERFORMANCE BASED ON SOZ PARAMETER DISTRIBUTION

periods	accuracy	sensitivity	specificity	AUC
pre-ictal	0.8308± 0.0580	0.7844± 0.0945	0.8772± 0.0699	0.9045± 0.0493
ictal	**0.9256± 0.0438**	**0.9139± 0.0643**	**0.9372± 0.0573**	**0.9720± 0.0263**
pre-ictal	0.8958± 0.0495	0.9072± 0.0670	0.8844± 0.0808	0.9485± 0.0347

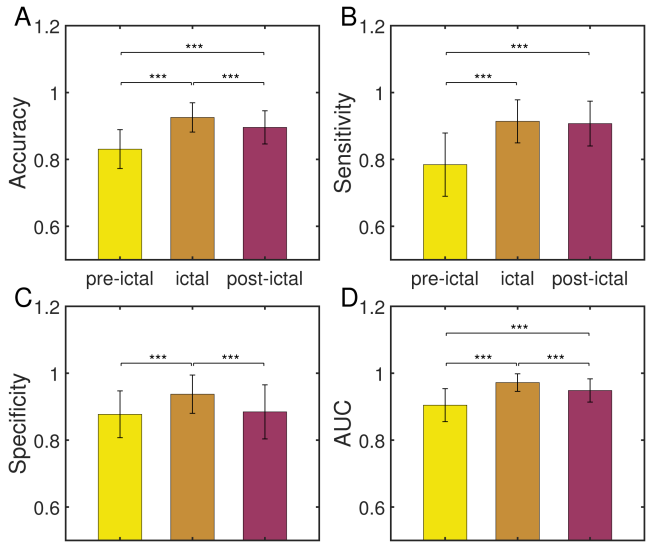

Fig. 10. Surgical outcomes classification performance based on SOZ parameter distribution. A, Accuracy. B, Sensitivity. C, Specificity. D, AUC. *** indicates $P<0.001$.

specificity (0.9454 ± 0.0666 and 0.9399 ± 0.0673), and AUC (0.9828 ± 0.0298 and 0.9872 ± 0.0213) compared to other conditions. These suggest that the presence of MRI-detected lesions may have influences on the SOZ localization.

Finally, to assess the ability of model parameter distribution to predict surgical outcomes, the SOZ model parameter distributions of patients with successful (13 patients) and unsuccessful (4 patients) surgeries are used as features to classify the surgical outcomes. The results, as shown in Table V and Fig. 10, indicate that all classification metrics during the ictal period are significantly higher than those during the pre-ictal and post-ictal periods, with the classification accuracy of surgical outcomes during the ictal period reaching as high as 0.9256 ($\pm$ 0.0438). These findings demonstrate the significant potential of using model parameter distribution as a feature for predicting surgical outcomes.

IV. DISCUSSION

Neural computational models are considered essential for simulating dynamic oscillations within the brain and studying the mechanisms of seizure onset and propagation. However, few studies have explored the application of model parameters in SOZ localization. In this study, the excitatory-inhibitory balance parameters of the Z6 model are estimated from the ECoG data of DRE patients using the UKF algorithm, with parameter distributions serving as classification features. SOZ localization is then performed using the bagging tree algorithm. The parameter estimation results indicate that the parameters generally follow a unimodal distribution during the pre-ictal and post-ictal periods, while they exhibit a bimodal distribution during the ictal period. Especially, differences can be easily observed between the peak values and corresponding parameters of SOZ and NSOZ distributions in three periods. The classification results demonstrate that the model based on parameter distribution can achieve excellent performance, with an average accuracy of 91.60% and an AUC of 96.43% . Furthermore, SOZ localization has also been performed using the parameter distribution in patients with and without MRI-detected lesions. The results indicate that the classification accuracy improves on patients without MRI-detected lesions. Additionally, the estimated parameter distributions have been used to predict epilepsy surgery outcomes, achieving a maximum average accuracy of 92.56% and an AUC of 97.20% . These findings suggest that the distribution of neural computational model parameters may complement existing SOZ localization and epilepsy surgery outcome prediction methods, providing a new perspective for clinical decision-making in epilepsy treatment.

Parameter distributions of neural computational models estimated by UKF might offer a novel approach for SOZ localization. In the current study, for pre-ictal, ictal and post-ictal periods, the SOZ classifications achieved a remarkable accuracy, which indicates that the model parameter distribution may contribute to accurately identifying SOZ. Furthermore, although the ECoG signals used in this study encompass various seizure onset patterns, the model parameters achieved good performance as classification features. This demonstrates the robustness of the model parameter estimation algorithm used in this study, highlighting its strong adaptability to different seizure onset patterns. Previous SOZ localization methods based on bioelectrical signals often focus more on analyzing and processing the signals themselves. For example, Jacobs et al. found that the rates of high-frequency oscillations (HFOs) are significantly higher in the SOZ, and the degree of post-spike high-frequency (HF) power attenuation in the SOZ is noticeably more severe compared to NSOZ regions [39]. Similarly, Du et al. proposed an SOZ localization algorithm based on multivariate HFO feature extraction and wavelet time-frequency maps, ultimately determining the SOZ classification results according to the wavelet time-frequency maps [11]. Additionally, Conrad et al. analyzed iEEG data from DRE patients and found that functional connectivity is reduced in the SOZ [40]. Unlike these previous studies, this study concentrates on the potential physiological significance of neural computational model parameters, which could more directly reflect the neurodynamic changes in the brain, and provide a possible underlying mechanism of seizures. Theoretically, the excitatory-inhibitory ratio is expected to be higher during the ictal period compared to the non-ictal period. The observed increase in the model parameter c during the ictal period is consistent with the theoretical expectation, emphasizing the physiological relevance of the model.

Also, as demonstrated in the current study, UKF-based parameter estimation has a strong performance in SOZ localization using pre-ictal, ictal and post-ictal data, which indicates that the method can capture not only abnormal neural activity during the ictal period but also potential alterations during the pre-ictal period. This capability may lay the foundation for early warning and intervention in epilepsy, highlighting its significant clinical application potential.

Theoretically, the core feature used for SOZ classification in this study is the parameter representing the balance between excitatory and inhibitory activity within brain regions. Indeed, extensive literature has demonstrated a close relationship between seizures and the imbalance between excitatory and inhibitory [41], [42].At the cellular and molecular levels, neurons promote the generation of action potentials by releasing excitatory neurotransmitters, such as glutamate [43], while inhibiting this process by releasing inhibitory neurotransmitters, such as GABAergic [44]. In epilepsy patients, excitatory activity is often excessively enhanced, while inhibitory function is weakened, and this imbalance is considered a primary trigger of seizure activity [45]. In the SOZ, this imbalance is particularly pronounced. Studies have shown that neurons in the SOZ tend to exhibit heightened excitatory activity, making them more prone to synchronized firing. This abnormal excitatory activity not only propagates within the SOZs but also spreads to adjacent NSOZs through axonal conduction, leading to the expansion of the seizure [46]. Notably, at the onset of seizures, low-voltage fast activity is commonly observed in neural signals, which may be related to the activation of inhibitory interneurons prior to excitatory neurons [47], [48]. Subsequently, as the overall excitability in the brain increases and inhibitory mechanisms weaken, ultimately resulting in a prolonged, large-amplitude epileptiform discharge. Therefore, the significant differences in the intensity and dynamics of excitatory and inhibitory activities between SOZs and NSOZs may underlie the effectiveness of balance parameters in localizing the SOZ.

The potential impact of different MRI lesion states on SOZ localization is explored in this study, and the results indicate that SOZ localization performs well regardless of the presence of MRI-detected lesions. However, higher classification accuracy is achieved when no lesions are observed on MRI. Unlikely, certain perspectives suggest that when lesions appear on the MRI of DRE patients, it generally aids in the localization of the SOZ [49], [50], [51]. This idea stems from the fact that structural abnormalities visible on MRI indicate potential sources of epileptic activity, making the SOZ more identifiable in clinical settings. Nevertheless, other studies highlight additional factors. For example, even though lesions are visible on MRI, only part of the lesion may correspond to the SOZ, while other parts could be areas adjacent to or connected with the SOZ within the epileptic network and influenced by it [52], [53]. This may lead to the incorrect identification of non-SOZ regions as SOZ. Moreover, not all SOZs present visible lesions on MRI, and some may have characteristics similar to other brain regions, making them harder to distinguish [54]. Despite ongoing debate regarding how MRI lesions influence SOZ localization, the UKF-based method relies mainly on the analysis of ECoG signals, showing minimal dependence on the presence of MRI-detected lesions. Thus, the presence or absence of MRI lesions has a limited impact on classification performance. Interestingly, the method is more sensitive to non-lesional signals, achieving relatively better SOZ localization in such cases.

Accurately predicting the outcome of epilepsy surgery holds significant importance in clinical practice for assessing surgical risks, aiding medical decision-making, and developing personalized surgical plans. Current studies on predicting epilepsy surgery outcomes utilize various approaches, including clinical and demographic features [55], graph theory metrics extracted from functional magnetic resonance imaging (fMRI) data [56], [57], and biomarkers such as interictal epileptiform discharges (IEDs) from EEG (or iEEG) signals [58]. Additionally, a combination of demographic, EEG, and MRI features has been applied to improve prediction accuracy [59], [60]. Furthermore, some studies employ physiological models fitted to invasive EEG recordings and adjust brain network models to simulate virtual resections of specific brain regions or connections, and the post-resection activity in these models is then analyzed to predict surgical outcomes [61], [62]. The aforementioned studies, by integrating various clinical information, biomarkers, and network model approaches, provide powerful tools for predicting epilepsy surgery outcomes. However, these methods still face certain limitations in simultaneously considering both temporal resolution and physiological interpretability. This study integrates estimated neural computational model parameters from the ECoG of DRE patients with machine learning techniques, preserving the high temporal resolution of ECoG signals and incorporating the physiological interpretability of neural models, demonstrating excellent predictive capabilities for surgical outcomes. Notably, these model parameter features are derived from ECoG signals recorded during epileptic periods prior to surgery, including the pre-ictal period, highlighting the potential of this method for clinical presurgical evaluation.

Despite the fact that the distributions of balance parameters estimated from ECoG signals in a neural computational model is firstly employed in the current study as classification features to localize the SOZs, several limitations must be acknowledged. First, this study selects ECoG data from only 13 DRE patients who undergo successful surgery, which may limit the generalizability of the results. Additionally, to maintain consistency in data processing, only ECoG data are considered, and SEEG data are not included. Despite that SEEG data also hold significant values, and future research on SOZ localization would incorporate SEEG data to enhance the applicability of the analysis and achieve better coverage of deep brain regions. Although high-frequency features of ECoG signals have garnered significant attention from researchers, this study primarily focuses on analyzing the frequency components within the 0.5–45 Hz range. Regarding the UKF algorithm, although it performs well in parameter estimation, the setting of process noise covariance and observation noise covariance may require multiple attempts to stabilize the algorithm, indicating a degree of dependence on experience. Finally, the Z6 model used in this study is based on simplified assumptions, which may not fully capture the complexity of biological systems. Therefore, future

studies should test the model on larger and diverse multicenter clinical datasets, consider employing models that better reflect physiological foundations to more accurately capture changes in brain neurodynamics, and explore methods for automating or adaptively adjusting the process and observation noise covariances in the UKF algorithm.

V. Conclusion

The excitatory-inhibitory balance parameter of the Z6 neural computational model is extracted from epileptic ECoG using the UKF algorithm, and SOZs have been accurately localized based on the distribution of this parameter. It is observed that the parameters follow a unimodal distribution during the pre-ictal and post-ictal periods, while the parameters exhibit a bimodal distribution during the ictal period. The classification model constructed using parameter distributions as features demonstrates excellent classification performance, with an average accuracy of 91.60% . Of note, the absence of MRI-detected lesions appears to contribute to improving classification performance. More importantly, the distribution of parameters significantly contributes to the prediction of epilepsy surgery outcomes, achieving an average accuracy of 92.56% . In summary, these findings suggest that the distribution of neural computational model parameters may serve as a biomarker for SOZ localization and epilepsy surgery outcome prediction, supporting medical decision-making in epilepsy treatment.

References

[1] J. Falco-Walter, "Epilepsy—Definition, classification, pathophysiology, and epidemiology," in *Seminars in Neurology*, vol. 40. New York City, NY, USA: Thieme Medical Publishers, Inc., 2020, pp. 617–623.

[2] R. Tsigebrhan et al., "Co-morbid mental health conditions in people with epilepsy and association with quality of life in low-and middle-income countries: A systematic review and meta-analysis," *Health Qual. Life Outcomes*, vol. 21, no. 1, 2023, Art. no. 5.

[3] N. M. Sayed, M. T. K. Aldin, S. E. Ali, and A. E. Hendi, "Cognitive functions and epilepsy-related characteristics in patients with generalized Tonic–Clonic epilepsy: A cross-sectional study," *Middle East Curr. Psychiatry*, vol. 30, no. 1, 2023, Art. no. 15.

[4] B. Mesraoua, F. Brigo, S. Lattanzi, B. Abou-Khalil, H. Al Hail, and A. A. Asadi-Pooya, "Drug-resistant epilepsy: Definition, pathophysiology, and management," *J. Neurological Sci.*, vol. 452, 2023, Art. no. 120766.

[5] H. Yan et al., "Deep brain stimulation for patients with refractory epilepsy: Nuclei selection and surgical outcome," *Front. Neurol.*, vol. 14, 2023, Art. no. 1169105.

[6] M. J. Morrell, "Responsive cortical stimulation for the treatment of medically intractable partial epilepsy," *Neurology*, vol. 77, no. 13, pp. 1295–1304, 2011.

[7] J. M. Bernabei et al., "Quantitative approaches to guide epilepsy surgery from intracranial eeg," *Brain*, vol. 146, no. 6, pp. 2248–2258, 2023.

[8] F. Rosenow and H. Lüders, "Presurgical evaluation of epilepsy," *Brain*, vol. 124, no. 9, pp. 1683–1700, 2001.

[9] A. Li et al., "Neural fragility as an eeg marker of the seizure onset zone," *Nature Neurosci.*, vol. 24, no. 10, pp. 1465–1474, 2021.

[10] H. Yu et al., "Variation of functional brain connectivity in epileptic seizures: An eeg analysis with cross-frequency phase synchronization," *Cogn. Neurodynamics*, vol. 14, pp. 35–49, 2020.

[11] Y. Du and B. Sun, "Accurate localization of seizure onset zones based on multi-feature extraction and wavelet time-frequency map," in *Proc. IEEE 37th Chin. Control Conf.*, 2018, pp. 4283–4288.

[12] W. Staljanssens et al., "Seizure onset zone localization from ictal high-density EEG in refractory focal epilepsy," *Brain Topogr.*, vol. 30, pp. 257–271, 2017.

[13] N. Rogers et al., "Correlation structure in micro-ECOG recordings is described by spatially coherent components," *PLoS Comput. Biol.*, vol. 15, no. 2, 2019, Art. no. e1006769.

[14] M. R. Mercier et al., "Advances in human intracranial electroencephalography research guidelines good practices," *Neuroimage*, vol. 260, 2022, Art. no. 119438.

[15] C. Yang, Q. Luo, H. Shu, R. L. B. Jeannès, J. Li, and W. Xiang, "Exploration of interictal to ictal transition in epileptic seizures using a neural mass model," *Cogn. Neurodynamics*, vol. 18, no. 3, pp. 1215–1225, 2024.

[16] Y. Shimoda et al., "Extracellular glutamate and gaba transients at the transition from interictal spiking to seizures," *Brain*, vol. 147, no. 3, pp. 1011–1024, 2024.

[17] Y. Yang et al., "Dynamic evolution of the anterior cingulate-insula network during seizures," *CNS Neurosci. Therapeutics*, vol. 29, no. 12, pp. 3901–3912, 2023.

[18] M. A. Hays et al., "Cortico-cortical evoked potentials in response to varying stimulation intensity improves seizure localization," *Clin. Neurophysiol.*, vol. 145, pp. 119–128, 2023.

[19] N. Wu and Y. Liu, "Least squares estimation of multifactor uncertain differential equations with applications to the stock market," *Symmetry*, vol. 16, no. 7, 2024, Art. no. 904.

[20] A. G. Roy and N. Peyada, "Lateral aircraft parameter estimation using neuro-fuzzy and genetic algorithm based method," in *Proc. 2017 IEEE Aerosp. Conf.*, 2017, pp. 1–11.

[21] N. J. Linden, B. Kramer, and P. Rangamani, "Bayesian parameter estimation for dynamical models in systems biology," *PLoS Comput. Biol.*, vol. 18, no. 10, 2022, Art. no. e1010651.

[22] X. Gao, X. Zhong, D. You, and S. Katayama, "Kalman filtering compensated by radial basis function neural network for seam tracking of laser welding," *IEEE Trans. Control Syst. Technol.*, vol. 21, no. 5, pp. 1916–1923, Sep. 2013.

[23] C.-H. Lee and J.-T. Chien, "Deep unfolding inference for supervised topic model," in *Proc. 2016 IEEE Int. Conf. Acoust., Speech Signal Process.*, 2016, pp. 2279–2283.

[24] X. Wen, D. Wang, L. Fan, Z. Lv, C. Zhang, and Z. Liang, "Tracking propofol-related brain states with UKF-based neural mass model," in *Proc. 41st Chin. Control Conf.*, 2022, pp. 5962–5966.

[25] B. Shan, J. Wang, B. Deng, X. Wei, H. Yu, and H. Li, "UKF-based closed loop iterative learning control of epileptiform wave in a neural mass model," *Cogn. Neurodynamics*, vol. 9, pp. 31–40, 2015.

[26] R. Fang, J. Wang, C. Liu, H. Yu, and Y. Qing, "Closed-loop control scheme to control epileptic activity based on UKF," in *Proc. IEEE 37th Chin. Control Conf.*, 2018, pp. 7980–7985.

[27] M. Çetin and S. Beyhan, "Adaptive stabilization of uncertain cortex dynamics under joint estimates and input constraints," *IEEE Trans. Circuits Syst. II: Exp. Briefs*, vol. 66, no. 4, pp. 627–631, Apr. 2019.

[28] A. Jafarian, D. R. Freestone, D. Nešić, and D. B. Grayden, "Slow-fast duffing neural mass model," in *Proc. IEEE 41st Annu. Int. Conf. Eng. Med. Biol. Soc.*, 2019, pp. 142–145.

[29] J. M. Bernabei et al., "Hup ieeg epilepsy dataset," OpenNeuro, 2023, doi: 10.18112/openneuro.ds004100.v1.1.3.

[30] J. Engel Jr, "Surgery for seizures," *New England J. Med.*, vol. 334, no. 10, pp. 647–653, 1996.

[31] A. Delorme and S. Makeig, "Eeglab: An open source toolbox for analysis of single-trial eeg dynamics including independent component analysis," *J. Neurosci. Methods*, vol. 134, no. 1, pp. 9–21, 2004.

[32] M. Koppert, S. Kalitzin, D. Velis, F. L. D. Silva, and M. A. Viergever, "Preventive and abortive strategies for stimulation based control of epilepsy: A computational model study," *Int. J. neural Syst.*, vol. 26, no. 08, 2016, Art. no. 1650028.

[33] S. Kalitzin, M. Koppert, G. Petkov, and F. L. D. Silva, "Multiple oscillatory states in models of collective neuronal dynamics," *Int. J. Neural Syst.*, vol. 24, no. 6, 2014, Art. no. 1450020.

[34] P. R. Bauer et al., "Dynamics of convulsive seizure termination and postictal generalized eeg suppression," *Brain*, vol. 140, no. 3, pp. 655–668, 2017.

[35] S. Julier, J. Uhlmann, and H. F. Durrant-Whyte, "A new method for the nonlinear transformation of means and covariances in filters and estimators," *IEEE Trans. Autom. Control*, vol. 45, no. 3, pp. 477–482, Mar. 2000.

[36] W.-Y. Loh, "Fifty years of classification and regression trees," *Int. Stat. Rev.*, vol. 82, no. 3, pp. 329–348, 2014.

[37] G. LemaÃŽtre, F. Nogueira, and C. K. Aridas, "Imbalanced-learn: A python toolbox to tackle the curse of imbalanced datasets in machine learning," *J. Mach. Learn. Res.*, vol. 18, no. 17, pp. 1–5, 2017.
[38] J. Huang and C. X. Ling, "Using AUC and accuracy in evaluating learning algorithms," *IEEE Trans. Knowl. Data Eng.*, vol. 17, no. 3, pp. 299–310, Mar. 2005.
[39] J. Jacobs, C. Vogt, P. L.Van, R. Zelmann, J. Gotman, and K. Kobayashi, "The identification of distinct high-frequency oscillations during spikes delineates the seizure onset zone better than high-frequency spectral power changes," *Clin. Neuriophysiol.*, vol. 127, no. 1, pp. 129–142, 2016.
[40] E. C. Conrad et al., "Addressing spatial bias in intracranial eeg functional connectivity analyses for epilepsy surgical planning," *J. Neural Eng.*, vol. 19, no. 5, 2022, Art. no. 056019.
[41] E. J. V. V. Hugte, D. Schubert, and N. N. Kasri, "Excitatory/inhibitory balance in epilepsies and neurodevelopmental disorders: Depolarizing γ-aminobutyric acid as a common mechanism," *Epilepsia*, vol. 64, no. 8, pp. 1975–1990, 2023.
[42] J. E. Niemeyer et al., "Seizures initiate in zones of relative hyperexcitation in a zebrafish epilepsy model," *Brain*, vol. 145, no. 7, pp. 2347–2360, 2022.
[43] H. I. Needs et al., "Changes in excitatory and inhibitory receptor expression and network activity during induction and establishment of epilepsy in the rat reduced intensity status epilepticus (rise) model," *Neuropharmacology*, vol. 158, 2019, Art. no. 107728.
[44] S. M. Sears and S. J. Hewett, "Influence of glutamate and GABA transport on brain excitatory/inhibitory balance," *Exp. Biol. Med.*, vol. 246, no. 9, pp. 1069–1083, 2021.
[45] Y. Wang, B. Tan, Y. Wang, and Z. Chen, "Cholinergic signaling, neural excitability, and epilepsy," *Molecules*, vol. 26, no. 8, 2021, Art. no. 2258.
[46] H. G. Meijer et al., "Modeling focal epileptic activity in the wilson–cowan model with depolarization block," *J. Math. Neurosci.*, vol. 5, pp. 1–17, 2015.
[47] F. Capitano et al., "Preictal dysfunctions of inhibitory interneurons paradoxically lead to their rebound hyperactivity and to low- voltage- fast onset seizures in Dravet syndrome," *Proc. Nat. Acad. Sci. USA*, vol. 121, no. 23, 2024, Art. no. e2316364121.
[48] M. de Curtis and M. Avoli, "Gabaergic networks jump-start focal seizures," *Epilepsia*, vol. 57, no. 5, pp. 679–687, 2016.
[49] Y. Tang et al., "Individual localization value of resting-state fmri in epilepsy presurgical evaluation: A combined study with stereo-EEG," *Clin. Neuriophysiol.*, vol. 132, no. 12, pp. 3197–3206, 2021.
[50] A. Berger et al., "Preoperative localization of seizure onset zones by magnetic source imaging, EEG-correlated functional MRI, and their combination," *J. Neurosurgery*, vol. 134, no. 4, pp. 1037–1043, 2020.
[51] J.-W. Jeong et al., "Multi-scale deep learning of clinically acquired multimodal mri improves the localization of seizure onset zone in children with drug-resistant epilepsy," *IEEE J. Biomed. Health Informat.*, vol. 26, no. 11, pp. 5529–5539, Nov. 2022.
[52] A. A. Asadi-Pooya, F. Brigo, S. Lattanzi, and I. Blumcke, "Adult epilepsy," *Lancet*, vol. 402, no. 10399, pp. 412–424, 2023.
[53] R. Shah, A. Botre, and V. Udani, "Trends in pediatric epilepsy surgery," *Indian J. Pediatrics*, vol. 82, pp. 277–285, 2015.
[54] L. Andrade-Valença et al., "Interictal high frequency oscillations (HFOS) in patients with focal epilepsy and normal MRI," *Clin. Neuriophysiol.*, vol. 123, no. 1, pp. 100–105, 2012.
[55] Z. Jourahmad et al., "Machine learning techniques for predicting the short-term outcome of resective surgery in lesional-drug resistance epilepsy," 2023, *arXiv:2302.10901*.
[56] S. Baxendale, "What are we really predicting with fMRI in epilepsy surgery?," *Epilepsy Behav.*, vol. 145, 2023, Art. no. 109298.
[57] B. C. Jobst and G. D. Cascino, "Thalamus as a 'hub' to predict outcome after epilepsy surgery," *Neurology*, vol. 88, no. 24, pp. 2246–2247, 2017.
[58] B. A. Dworetzky and C. Reinsberger, "The role of the interictal eeg in selecting candidates for resective epilepsy surgery," *Epilepsy Behav.*, vol. 20, no. 2, pp. 167–171, 2011.
[59] Z. Fitzgerald et al., "Improving the prediction of epilepsy surgery outcomes using basic scalp eeg findings," *Epilepsia*, vol. 62, no. 10, pp. 2439–2450, 2021.
[60] C. Tonini et al., "Predictors of epilepsy surgery outcome: A meta-analysis," *Epilepsy Res.*, vol. 62, no. 1, pp. 75–87, 2004.
[61] A. P. Millán et al., "Epidemic models characterize seizure propagation and the effects of epilepsy surgery in individualized brain networks based on MEG and invasive EEG recordings," *Sci. Rep.*, vol. 12, no. 1, 2022, Art. no. 4086.
[62] A. P. Millán et al., "Individualized epidemic spreading models predict epilepsy surgery outcomes: A pseudo-prospective study," *Netw. Neurosci.*, vol. 8, no. 2, pp. 437–465, 2024.